Knee cartilage segmentation using active shape models and local binary patterns

Germán González[a] and Boris Escalante-Ramírez[b]

[a]Posgrado en Ingeniería Eléctrica, Universidad Nacional Autónoma de México, Mexico City, Mexico;
[b]Departamento de Procesamiento de Señales, Facultad de Ingeniería, Universidad Nacional Autónoma de México, Mexico City, Mexico

ABSTRACT

Segmentation of knee cartilage has been useful for opportune diagnosis and treatment of osteoarthritis (OA). This paper presents a semiautomatic segmentation technique based on Active Shape Models (ASM) combined with Local Binary Patterns (LBP) and its approaches to describe the surrounding texture of femoral cartilage. The proposed technique is tested on a 16-image database of different patients and it is validated through Leave-One-Out method. We compare different segmentation techniques: ASM-LBP, ASM-medianLBP, and ASM proposed by Cootes. The ASM-LBP approaches are tested with different ratios to decide which of them describes the cartilage texture better. The results show that ASM-medianLBP has better performance than ASM-LBP and ASM. Furthermore, we add a routine which improves the robustness versus two principal problems: over-segmentation and initialization.

Keywords: Knee Cartilage, Segmentation, active shape models, local binary patterns

1. INTRODUCTION

Knee Osteoarthritis (OA)[1] is one of the most frequent diseases around the world which causes pain, malfunction and disability. OA is caused by biomechanical stress that affects knee articular cartilages and bones. OA may be present in any of the medial femoral compartments, either the tibiofemoral or patellofemoral, according to the location of damaged cartilage. Pain, morning stiffness and knee swelling in a patient older than 50 years are considered OA consequences. Moreover, image analysis of the knee has an important role since it confirms the OA diagnosis, determines which compartments have been affected and determines the disease stage. Image analysis can also confirm the responsibility of OA on the symptoms and provides information about disease evolution during treatment. In this case, Magnetic Resonance Imaging (MRI) can show the soft tissue structures and their boundaries with the bones, without significant distortion. Furthermore, MRI does not change the dimension of tissues and there is not superposition between anatomical structures and, most important, it directly visualizes the knee cartilage and its defects.

Taking advantage of MRI characteristics, we can extract regions of interest (segmentation) from these images, in our case, knee cartilage. Automatic or semiautomatic knee cartilage segmentation has been studied for more than 20 years and many approaches have been reported, for example: growing regions,[2] active contours,[3] Bayesian classifiers[4] and active shape models.[5] The **Active Shape Models (ASM)**[6] compute an average shape of the region of interest from a training set and a statistical model of minimal parameters that allow the shape to adjust to different objects within a certain range. ASM have been widely used in medical image analysis because there is sufficient knowledge about the shape of anatomical structures, which are obtained through diverse medical imaging modes.

The ASM use an appearance model based on local gray profiles to describe the region around the structure of interest. These profiles have shown not so great robustness in practice, to overcome this issue, some authors have

Further author information: (Send correspondence to G. G.)
G.G.: E-mail: germangs999@gmail.com
B.E.: E-mail: boris@unam.mx, Telephone: (52) 55-56161719

Optics, Photonics, and Digital Technologies for Multimedia Applications III, edited by Peter Schelkens, Touradj Ebrahimi, Gabriel Cristóbal, Frédéric Truchetet, Pasi Saarikko, Proc. of SPIE Vol. 9138, 91380K · © 2014 SPIE · CCC code: 0277-786X/14/$18 · doi: 10.1117/12.2054783

improved the appearance model adding different image processing techniques, i.e.: multiresolution,[7] non-linear classifiers and gradients,[8] probabilistic estimation,[9] locally order-less images,[10] and rotation invariant locally order-less images.[11] This paper proposes to use the texture descriptor called **Local Binary Patterns (LBP**) to obtain a new appearance model for ASM.[12] The LBP describe the region around the landmarks and shape adjustment is calculated by a similarity measure (ASM uses Mahalanobis distance) between histograms. The ASM with LBP have shown better results than original ASM.

This paper is organized as follows: Section 2 is devoted to describe the ASM algorithm, LBP approaches, ASM with LBP algorithm and segmentation validation. Later, in Section 3, image database and presegmentation routine are described and we show our results with the improvements obtained. Finally, the conclusions are drawn in Section 4.

2. METHODS

2.1 Active Shape Models

The Active Shape Model (ASM) is a combined technique of Point Distribution Model (PDM) and iterative template deformation and it was originally described by Cootes *et al.*[6]

- **Training phase.** A training set of medical images with annotated shapes or regions of interest (by an expert) is necessary for this phase, they are marked with the same number of points, called landmarks. The shapes are aligned between themselves using pose transformations (scale, rotation and translation) and the mean shape $\bar{X}$ is calculated from the aligned set of shapes.

  The PDM is built applying Principal Component Analysis (PCA) to the aligned set. The original shapes X_i and their representation model $b_i (i = 1, ..., N)$, N is the number of variation modes, are related by the mean shape $\bar{X}$ and the eigenvectors P:

$$X_i = \bar{X} + Pb_i. \tag{1}$$

  The representation dimensionality is reduced using only the eigenvectors of the major eigenvalues. In this case, equation 1 turns into an approximation, with an error depending on the magnitude of the excluded eigenvalues.

- **Pose Adjustment.** PDM can be used for generating new shapes similar to those in the training set by modifying b, within certain limits.

  Assuming that a shape model is described as the sum of the mean shape obtained from the training set and the weighted sum of the principal components, with the possibility of being translated, rotated, and scaled, then, the expression of the initial estimation x_1 of a shape as a scaled, rotated and translated version of reference shape x_2 is:

$$x_1 = M(s_1, \theta_1)[x_2] + t_1, \tag{2}$$

  where $M(s, \theta) = \begin{pmatrix} (s)\cos(\theta) & -(s)\sin(\theta) \\ (s)\sin(\theta) & (s)\cos(\theta) \end{pmatrix}$ and $t_1 = (t_{x1}, t_{y1} ... t_{x1}, t_{y1})^T$.

  The shape x_2 is expressed as $x_1 = \bar{x} + dx_2$, where $dx_2 = Pb_2$. Hence, the initial estimation is $x_1 = M(s_1, \theta_1)[\bar{x} + dx_2] + t_1$. Fitting the initial estimation to image data is necessary. A new location $x_1 + dx_1$ is obtained by examining the surrounding region of each landmark of x_1.

  Afterwards, the pose parameters (scaling, rotation and translation) are adjusted, as well as the shape parameters (the weights of the principal components) to move our current estimate x_1 as close as possible to $x_1 + dx_1$, considering that the form is acceptable. So, the additional scaling $1 + ds$, rotation $d\theta$ and translation (dt_x, dt_y) is required to move x_1 as close as possible to $x_1 + dx_1$:

$$M(s_1(1 + ds), \theta_1 + d\theta)[x_2] + (t_1 + dt) \longrightarrow x_1 + dx_1. \tag{3}$$

  There are remaining adjustments which can only be satisfied by deforming the shape x_2.

- **Appearance Model.** The appearance model is described by gray level statistics around each landmark and gives us adjustment information to fit the model. To find such adjustments, we search along a line passing through the landmark and perpendicular to the boundary formed by the landmark and its neighbors.

  The search profile is obtained from gray level values along the profile and compute its derivative and normalization. The normalized derivative search profile is:

$$y_{si} = \frac{ds_i}{\sum_{k=1}^{t_s-1} |ds_{ik}|}, \tag{4}$$

  where gray level profile is $s_i = [s_{i1}\, s_{i2} \ldots s_{i(t_s)}]$, and i refers to i-th landmark.

  The landmark moves to the position where the most similar sub-profile to mean normalized derivative profile is found. That similarity is calculated with the following square error function, called Mahalanobis Distance:

$$f(p_p) = (p_p - \bar{p})^T C_p^{-1} (p_p - \bar{p}), \tag{5}$$

  where C_p^{-1} is the inverse covariance matrix of the mean normalized derivative gray profile $\bar{p}$ and p_p is the sub-profile. The suggested position of dX_i is where $f(p_p)$ is minimum.

  The total suggested displacement obtained from the appearance model is:

$$dX = (dX_0,\, dY_0,\, \ldots dX_{n-1},\, dY_{n-1})^T. \tag{6}$$

- **Shape Adjustment.** Knowing $1 + ds$, $d\theta$ and dt, we find the shape adjustment through dx:

$$dx = M((s_i(1+ds))^{-1}, -(\theta_i + d\theta))[M(s_i, \theta_i)[x_l] + dX - dt] - x_l. \tag{7}$$

  Equation (7) estimates the adjustments for x_l. Afterwards, we calculate $d\mathbf{b}$ by the equation:

$$d\mathbf{b} = P^T dx. \tag{8}$$

  But, sometimes, these adjustments are not consistent with the shape model, then, the update $b \to b + db$ is verified with:

$$-A\sqrt{\lambda_k} \leq b_k \leq A\sqrt{\lambda_k}, \tag{9}$$

  where A is constant (Cootes *et al.*[6] proposed $A = 3$).

Finally, if the condition is valid, shape and pose parameters are updated as follows:

$$\begin{aligned} t_x + dt_x &\to t_x \\ t_y + dt_y &\to t_y \\ t_\theta + dt_\theta &\to \theta \\ s(1+ds) &\to s \\ b + db &\to b \end{aligned} \tag{10}$$

The process is repeated for a number of iterations.

2.2 Local Binary Patterns

The original Local Binary Pattern (LBP) descriptor[13] was proposed by Ojala *et al.* based on the idea is that textural properties within homogeneous regions can be translated into patterns, these patterns represent local features. The original LBP uses a 3×3 mask to describe the neighborhood around a central pixel. The gray intensity values of neighboring pixels are compared with the central pixel; those values lesser than the central pixel value are labeled with "0", otherwise, they are labeled with "1". The labels are multiplied by a weighting function according with their positions to form a chain (pattern). Later, the sum of those eight values replaces the value of the central pixel. As we can see, this method is based on differences of intensities and produces 2^8 possible values.

Further generalizations use a circular neighborhood instead of a fixed region. The sampling coordinates are calculated using the expression:

$$x_p = x + R\cos(2\pi p/P) \tag{11}$$

$$y_p = y - R\sin(2\pi p/P), \tag{12}$$

where $g_p = I(x_p, y_p)$ is the central pixel intensity of the uniformly spaced circular region with P sample points and ratio R around the central pixel. With this implementation, we could change the spatial resolution and the number of sampling points easily. The LBP expression is:

$$LBP_{P,R}(x_c, y_c) = \sum_{p=0}^{P-1} s(g_p - g_c)2^P. \tag{13}$$

where $s(z)$ is defined as:

$$s(z) = \begin{cases} 1, & z \geq 0, \\ 0, & z < 0. \end{cases} \tag{14}$$

The **median LBP**[14] was proposed by Zabih and it is less sensitive to noise. The median LBP replaces the central pixel with the media of itself and the P neighbors. The expression of median LBP is:

$$LBP^{med}_{P,R}(x_c, y_c) = \sum_{p=0}^{P-1} s(g_p - \bar{g}), \tag{15}$$

where $\bar{g}$ represents the median of the P neighbors and the central pixel. This modification is still invariant to rotation but less sensitive to noise. It is also invariant to monotonic illumination changes.

2.3 Active Shape Models with Local Binary Patterns

The segmentation algorithm is based on *Divided-Square-based LBP-ASM* reported by Keomany *et al.*[12] The authors used a $LBP_{8,2}$ operator.

On the training phase, the LBP histogram (appearance model) is extracted from each landmark by concatenating the four sub-regions LBP histograms (Figure 1). Afterwards, a mean LBP histogram is calculated from the LBP histograms from each landmark. The LBP histogram substitutes the local gray profiles of the original ASM, however, the statistical model (mean shape, eigenvalues and eigenvectors) remains the same as it was calculated by PCA.

On the segmentation phase, the shape adjustment is obtained as follows:

1. Normal-oriented points are obtained from each landmark and they are used as square sub-regions centers.
2. LBP histogram are calculated at each point previously acquired.

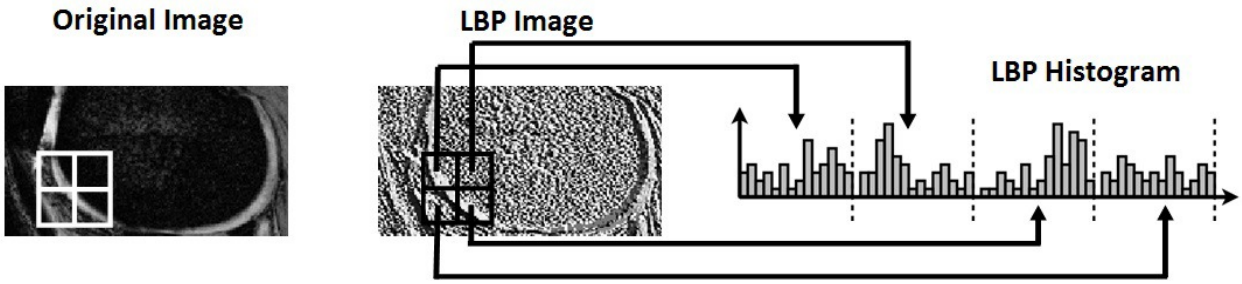

Figure 1. Local appearance model from sub-regions histogram.

3. Calculated LBP histograms are compared with the mean LBP histogram for each landmark with *Chi square* statistic. Chi square substitutes the Mahalanobis distance (equation 5) on the original ASM scheme and it is defined as:

$$\chi^2(H, \bar{H}) = \sum_i \frac{(H_i - \bar{H}_i)^2}{(H_i + \bar{H}_i)}, \tag{16}$$

where i refers to the i-th landmark, H_i is the LBP histogram from a normal point (step 2) and $\bar{H}$ is the mean LBP histogram. The smaller the Chi square is, more similar the histograms are.

4. The new landmark position (dX) is found where the similarity is the greatest. Pose and shape parameters are adjusted (dx) as in the original ASM.

Finally, ASM with LBP offer interesting properties: pixel level information from LBP descriptor, spatial information from sub-regions histograms and global information from concatenated LBP histograms.

2.4 Validation

We validate the accuracy of our segmentation algorithm with two different measures: DICE coefficient and Hausdorff distance.

2.4.1 DICE Coefficient

The DICE coefficient is a similarity measurement between sets. In this case, it is used as a global measure of the existing differences between the calculated shape and the reference shape. The coefficient is given by:

$$DICE = \frac{2(A \cap B)}{|A| + |B|}, \tag{17}$$

where A is the area inside the calculated shape and B is the area inside the reference shape. DICE coefficient values are between 0 and 1; the closer the coefficient to 1, the more similar the shapes are.

2.4.2 Hausdorff Distance

The Hausdorff distance determines the similarity between two shapes.[15] The Hausdorff distance is defined as the maximum distance from a point set to the nearest point of another point-set. The Hausdorff distance between A and B point-sets is:

$$H(A, B) = max(h(A, B), h(B, A)), \tag{18}$$

where:

$$h(A, B) = max_(a \in A) min_(b \in B) \|a - b\|. \tag{19}$$

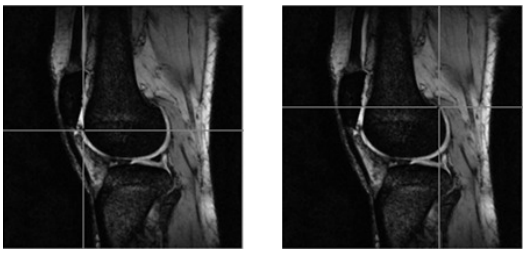

Figure 2. Points for presegmentation routine.

The equation 19 is called the direct Hausdorff distance from the set A to set B, using the underlying norm $\|\cdot\|$ on the point sets A and B, and

$$h(B,A) = max_(b \in B)min_(a \in A)\|b-a\| \tag{20}$$

is called inverse Hausdorff distance. The Hausdorff distance is not symmetric. Then, equation 18 considers both cases giving a more general definition.

3. RESULTS

3.1 Medical Image Dataset

The images were selected from 16 different volume sets on a 3T MRI system (Siemens Verio). The images are in T2 in an echo-time series (Multi-echo system). The image parameters are: TR = 960 ms, TE = 7.54 ms, and flip angle = 60. The images were acquired with a 384 × 384 × 10 matrix (0.414-mm in-plane resolution and 3.6-mm slice thickness).

3.2 Presegmentation Routine

We propose the following presegmentation routine to improve segmentation results:

- Mark two important points: the left and right inside corners of knee cartilage (Figure 2).
- Obtain the distance between these points ($dist_A$) and the distance between their equivalent points on the mean shape $\bar{X}$, calculated in the training phase ($dist_B$). A proportional measure is obtained from these distances and it is defined as:

$$s = \frac{dist_A}{dist_B}. \tag{21}$$

The value s is a scale parameter that multiplies the mean shape $\bar{X}$ before the adjustment of pose and shape parameters:

$$\bar{X}_{new} = \begin{bmatrix} 0.9s & 0 \\ 0 & 0.9s \end{bmatrix} \bar{X}, \tag{22}$$

where $\bar{X}_{new}$ is the updated mean shape. Based on experimentation, we propose the constant 0.9.

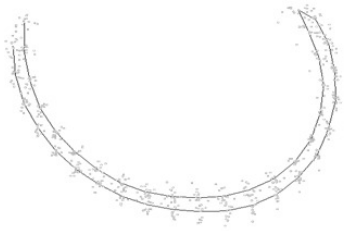

Figure 3. The mean shape and the sample points of aligned training shapes.

3.3 Experimental Results

Since the ASM require prior training, we used the "leave-one-out" method to maximize data usage. The DICE coefficient and Hausdorff distance are metrics used for validating the segmentation results. The shapes are 42-point contours. The original ASM, the mean and sub profiles length is 7 pixels and the test profile length is 17 pixels (11 comparisons are done for each landmark). For ASM-LBP, the test profile length is 9 pixels and the square sub-regions size is 5×5 pixels. Figure 3 shows the mean shape and the sample points of aligned training shapes.

The two relevant image points of Section 3.2 are used as fixed points on equation (6) in every iteration. This consideration provides faster convergence, better adjustment, and avoids over-segmentation which tends to patellae cartilage.

The proposal was evaluated on 16 knee cartilage images using the Original ASM, ASM-LBP and ASM-medianLBP with square subregions described on Section 2.3. Both ASM-LBP algorithms were tested with the same sample points ($P = 8$) and five different ratios (R): 1, 2, 3, 5 and 10. The best results of DICE coefficient are shown on Table 1 and the best results of Hausdorff distance are shown in Table 2. The best results for each image are in bold font.

The best results are not consistent and they do not lead us to decide which one is better. For that reason, we evaluated the algorithms using various initialization points for each image. Table 3 shows both mean DICE and mean Hausdorff distance results, with standard deviation, for each image, and, at the bottom of each validation metric, it shows the mean results for each segmentation algorithm. The best results are in bold font.

This last evaluation shows that ASM-LBP has better results than Original ASM. For the DICE coefficient, ASM-LBP and ASM-medianLBP, with ratio 1 and 2, have better mean results than the others. For the Hausdorff distance, ASM-medianLBP, with ratio 1 and 2, have the better mean results. More precisely, $ASMLBP^{med}_{8,2}$ has the best mean DICE result, but, $ASMLBP^{med}_{8,1}$ has the best mean Hausdorff distance result.

Apparently, there is no difference between choosing any of them, but, we use ANOVA (*Analysis of Variance*) to decide which one is better: $ASMLBP^{med}_{8,1}$ or $ASMLBP^{med}_{8,2}$. More precisely, ANOVA indicates if a significant difference already exists between choosing one of them or we could expect a similar result choosing any of them. The ANOVA of DICE coefficient shows no significant difference between them ($Prob > F = 0.2047$). But, ANOVA of Hausdorff distance shows there a significant difference between them ($Prob > F = 7.0240e^{-12}$). Considering normal-distributed data, the mean and standard deviation of Hausdorff distance of $ASMLBP^{med}_{8,1}$ are 3.0709 ± 1.0552, and of $ASMLBP^{med}_{8,2}$ are 3.2007 ± 1.4841, moreover, the number of outliers (samples out of the mean and standard deviation) are: 680 for $ASMLBP^{med}_{8,1}$ and 816 for $ASMLBP^{med}_{8,2}$. Therefore, $LBP^{med}_{8,1}$ is the best texture descriptor for the ASM-LBP algorithm due to its lower mean Hausdorff distance, variance and number of outliers. The best results for images 2, 5 ,6, 10, 13 and 14 are shown in Figure 4.

4. CONCLUSIONS

In this paper, we proposed a segmentation algorithm based on ASM that uses the texture descriptor LBP to obtain a better knee cartilage segmentation, and, we compared it with the original ASM. For ASM-LBP, we use two different LBP approaches: Original LBP and median LBP. Moreover, we tested LBP approaches with

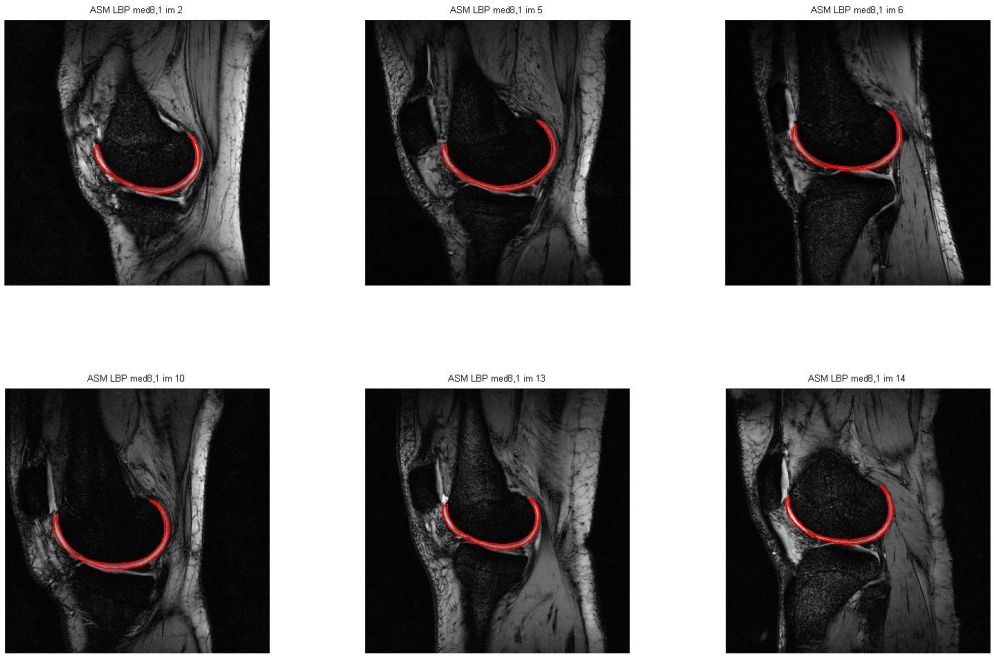

Figure 4. The best segmentation results with $ASMLBP^{med}_{8,1}$.

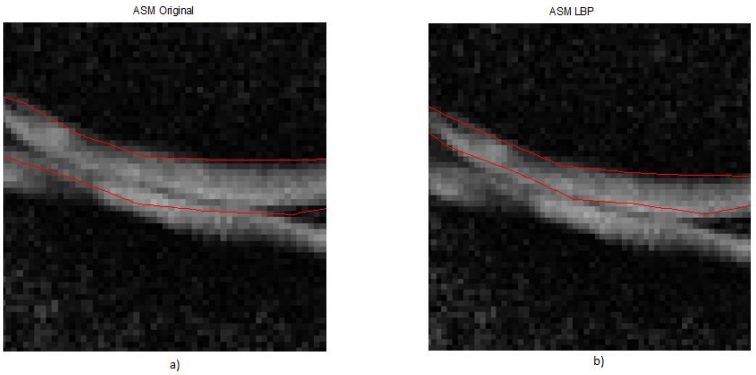

Figure 5. a) Oversegmentation problem of ASM, b) Oversegmentation robustness of ASM-LBP

different ratios ($R = 1, 2, 3, 5$ and 10) with the same sample points ($P = 8$) in order to determine the best knee cartilage descriptor. We also tested with different initialization points in order to avoid the problem of user's initialization. Based on mean results and their variance, we conclude that $ASMLBP^{med}_{8,1}$ has the best segmentation results, second, and close to it, $ASMLBP^{med}_{8,2}$, and lastly, the other ASM-LBP algorithms which also show better results than the original ASM.

The ASM-LBP also provides better segmentation robustness than ASM due to the properties mentioned in Section 2.3. Figure 5.a shows the over-segmentation problem of tibial cartilage using ASM and 5.b shows ASM-LBP improved robustness to that problem. Moreover, in Section 3.3, we discussed the robustness to the over-segmentation of patellae cartilage due to the presegmentation routine in Section 3.2.

Further research will be devoted to test the algorithm with different data, and to design relaxometry studies taking advantage of magnetic resonance and image acquisition.

5. ACKNOWLEDGMENTS

We would like to thank Ph.D. Marcelo F. Lugo-Licona for his helpful comments and the departments of Magnetic Resonance and Radiotherapy of the Hospital Ángeles de las Lomas for providing MR Images. The authors greatly acknowledge the support by research grants from UNAM PAPIIT IG100814 and CONACYT-325545.

REFERENCES

[1] Bonnin, M. and Chambat, P., [*Osteoarthritis of the Knee*], Springer (2008).
[2] Eckstein, F., Cicuttini, F., Raynauld, J.-P., Waterton, J., and Peterfy, C., "Magnetic resonance imaging (mri) of articular cartilage in knee osteoarthritis (oa): morphological assessment," *Osteoarthritis and cartilage* **14**, 46–75 (2006).
[3] Raynauld, J.-P., Kauffmann, C., Beaudoin, G., Berthiaume, M.-J., de Guise, J., Bloch, D., Camacho, F., Godbout, B., Altman, R., Hochberg, M., et al., "Reliability of a quantification imaging system using magnetic resonance images to measure cartilage thickness and volume in human normal and osteoarthritic knees," *Osteoarthritis and cartilage* **11**(5), 351–360 (2003).
[4] Kapur, T., Beardsley, P., Gibson, S., Grimson, W., and Wells, W., "Model-based segmentation of clinical knee mri," in [*Proc. IEEE Intl Workshop on Model-Based 3D Image Analysis*], 97–106, Citeseer (1998).
[5] Solloway, S., Hutchinson, C. E., Waterton, J. C., and Taylor, C. J., "The use of active shape models for making thickness measurements of articular cartilage from mr images," *Magnetic Resonance in Medicine* **37**(6), 943–952 (1997).
[6] Cootes, T. F., Taylor, C. J., Cooper, D. H., and Graham, J., "Active shape models-their training and application," *Computer vision and image understanding* **61**(1), 38–59 (1995).
[7] Abu-Gharbieh, R., Hamarneh, G., and Gustavsson, T., "Review-active shape models-part ii: Image search and classification," in [*In Proc. Swedish Symposium on Image Analysis*], Citeseer (1998).
[8] Li, S., Zhu, L., and Jiang, T., "Active shape model segmentation using local edge structures and adaboost," in [*Medical Imaging and Augmented Reality*], 121–128, Springer (2004).
[9] Chen, Y., Cai, X., and Sowmya, A., "Boosted dynamic active shape model," in [*Image and Vision Computing New Zealand, 2009. IVCNZ'09. 24th International Conference*], 215–220, IEEE (2009).
[10] Van Ginneken, B., Frangi, A. F., Staal, J. J., ter Haar Romeny, B. M., and Viergever, M. A., "Active shape model segmentation with optimal features," *medical Imaging, IEEE Transactions on* **21**(8), 924–933 (2002).
[11] Ordas, S., Boisrobert, L., Huguet, M., and Frangi, A., "Active shape models with invariant optimal features (iof-asm) application to cardiac mri segmentation," in [*Computers in Cardiology, 2003*], 633–636, IEEE (2003).
[12] Keomany, J., Marcel, S., et al., "Active shape models using local binary patterns," (2006).
[13] Ojala, T., Pietikäinen, M., and Harwood, D., "A comparative study of texture measures with classification based on featured distributions," *Pattern recognition* **29**(1), 51–59 (1996).
[14] Zabih, R. and Woodfill, J., "Non-parametric local transforms for computing visual correspondence," in [*Computer VisionECCV 94*], 151–158, Springer (1994).
[15] Huttenlocher, D. P., Klanderman, G. A., and Rucklidge, W. J., "Comparing images using the hausdorff distance," *Pattern Analysis and Machine Intelligence, IEEE Transactions on* **15**(9), 850–863 (1993).

Img	ASM	$ASMLBP_{8,1}$	$ASMLBP_{8,2}$	$ASMLBP_{8,3}$	$ASMLBP_{8,5}$	$ASMLBP_{8,10}$	$ASMLBP^{med}_{8,1}$	$ASMLBP^{med}_{8,2}$	$ASMLBP^{med}_{8,3}$	$ASMLBP^{med}_{8,5}$	$ASMLBP^{med}_{8,10}$
1	0.8293	0.8413	0.8421	0.8435	0.8355	0.8300	0.8414	**0.8500**	0.8498	0.8350	0.8436
2	0.8379	0.8928	0.9079	**0.9111**	0.8838	0.8885	0.9009	0.9019	0.9061	0.8921	0.9059
3	**0.9020**	0.8617	0.8660	0.8761	0.8526	0.8501	0.8626	0.8688	0.8682	0.8672	0.8497
4	**0.8549**	0.8493	0.8494	0.8391	0.8361	0.8502	0.8478	0.8532	0.8538	0.8536	0.8538
5	0.8764	0.8885	0.8946	0.8849	0.8752	0.8685	0.8828	**0.8993**	0.8889	0.8859	0.8860
6	0.8579	0.8802	0.8824	**0.8857**	0.8552	0.8581	0.8849	0.8847	0.8832	0.8612	0.8597
7	**0.8648**	0.8473	0.8433	0.8523	0.8216	0.8293	0.8374	0.8405	0.8450	0.8249	0.8313
8	0.8293	0.8478	0.8477	0.8487	0.8390	0.8400	0.8472	**0.8517**	0.8488	0.8363	0.8375
9	**0.8826**	0.8382	0.8535	0.8554	0.8508	0.8503	0.8488	0.8534	0.8581	0.8728	0.8495
10	**0.9276**	0.8848	0.9021	0.9014	0.8920	0.8818	0.8809	0.8935	0.9032	0.8893	0.8565
11	0.8794	0.8650	0.8727	**0.8825**	0.8792	0.8723	0.8603	0.8782	0.8783	0.8690	0.8270
12	0.8667	0.8590	**0.8636**	0.8611	0.8411	0.8449	0.8564	0.8605	0.8644	0.8544	0.8453
13	0.8903	0.9190	0.9116	0.9148	0.9197	0.9024	0.9076	0.9127	**0.9207**	0.9063	0.8807
14	0.8806	0.8886	0.8902	0.8823	0.8793	0.8815	**0.8911**	0.8854	0.8759	0.8887	0.8745
15	0.8968	0.9003	0.9088	0.9125	0.9018	**0.9131**	0.8886	0.8927	0.9082	0.9111	0.8988
16	**0.9151**	0.8590	0.8628	0.8817	0.8832	0.8696	0.8570	0.8607	0.8859	0.8785	0.8527

Table 1. The best DICE results for each image of dataset.

Img	ASM	$ASMLBP_{8,1}$	$ASMLBP_{8,2}$	$ASMLBP_{8,3}$	$ASMLBP_{8,5}$	$ASMLBP_{8,10}$	$ASMLBP^{med}_{8,1}$	$ASMLBP^{med}_{8,2}$	$ASMLBP^{med}_{8,3}$	$ASMLBP^{med}_{8,5}$	$ASMLBP^{med}_{8,10}$
1	2.0164	1.9746	**1.8705**	1.9711	1.9936	2.0865	1.9275	1.9416	2.0362	2.0707	2.1645
2	2.3684	2.2222	**2.1613**	2.3390	2.4099	2.3916	2.2292	2.2922	2.3048	2.4087	2.3009
3	**1.8009**	2.1835	1.9452	1.9620	2.3897	2.2123	2.1355	2.0566	1.8951	2.2512	2.1638
4	2.4534	2.3661	2.4131	2.4145	2.4544	2.3541	**2.2664**	2.4136	2.4018	2.3737	2.3514
5	**2.1965**	2.3220	2.3317	2.3225	2.2687	2.4260	2.3609	2.4488	2.3665	2.4340	2.3583
6	**1.4607**	2.5404	2.5752	2.5430	2.6093	2.6697	2.6037	2.5662	2.6028	2.5103	2.5561
7	**1.7901**	1.8219	2.0803	2.4639	2.6183	2.4138	1.9709	2.1367	2.4486	2.5263	2.3698
8	2.0053	1.8315	1.4281	**1.3734**	2.1961	1.6666	1.8292	1.6558	1.4430	1.3962	1.6946
9	2.4600	2.2204	2.1548	2.1164	**1.9683**	2.2515	2.1351	2.1097	2.0788	2.0003	2.1541
10	**1.4230**	2.6784	2.5740	2.7179	2.7233	2.8999	2.5368	2.4450	2.5409	2.6718	2.5464
11	**1.4828**	3.1931	3.3516	3.2309	3.3602	3.3781	2.5465	3.2842	2.9062	2.8430	3.0074
12	3.3186	**2.0757**	2.2169	2.3221	2.3832	2.3246	2.1284	2.2478	2.2794	2.0877	2.2670
13	1.2402	**1.1832**	1.4420	1.3341	1.3901	1.4042	1.2575	1.3867	1.2372	1.3068	1.4234
14	2.4919	**2.1028**	2.2080	2.1396	2.4083	2.2297	2.1918	2.1759	2.1764	2.2305	2.2945
15	2.3197	2.0666	2.0634	2.2051	2.1725	2.2342	2.1762	2.2615	2.1291	2.3012	**2.0094**
16	**1.6485**	1.8485	1.8769	1.9737	2.2863	2.2442	1.8579	1.8746	1.8647	1.8638	2.0431

Table 2. The best HAUSDORFF DISTANCE results for each image of dataset.

Proc. of SPIE Vol. 91380K-11

Img	ASM	$ASMLBP_{8,1}$	$ASMLBP_{8,2}$	$ASMLBP_{8,3}$	$ASMLBP_{8,5}$	$ASMLBP_{8,10}$	$ASMLBP^{med}_{8,1}$	$ASMLBP^{med}_{8,2}$	$ASMLBP^{med}_{8,3}$	$ASMLBP^{med}_{8,5}$	$ASMLBP^{med}_{8,10}$
1	0.636 ± 0.1759	0.77568 ± 0.1258	0.78816 ± 0.083407	0.71435 ± 0.19054	0.59199 ± 0.25376	0.58654 ± 0.27058	0.80451 ± 0.066465	**0.81015 ± 0.051328**	0.78337 ± 0.10903	0.66071 ± 0.23259	0.73054 ± 0.17462
2	0.7234 ± 0.0669	0.83135 ± 0.092878	**0.86266 ± 0.069035**	0.8439 ± 0.099131	0.76222 ± 0.16067	0.79935 ± 0.14788	0.83949 ± 0.086287	0.85981 ± 0.069135	0.85261 ± 0.075097	0.8219 ± 0.1105	0.8615 ± 0.070179
3	0.7371 ± 0.1552	**0.8167 ± 0.04444**	0.78732 ± 0.12091	0.72889 ± 0.20374	0.51289 ± 0.25149	0.62294 ± 0.19668	0.8141 ± 0.047245	0.79568 ± 0.12297	0.80313 ± 0.10952	0.67014 ± 0.17693	0.67907 ± 0.13101
4	0.613 ± 0.2300	0.81095 ± 0.066537	0.79497 ± 0.096837	0.61152 ± 0.22017	0.4977 ± 0.27148	0.55647 ± 0.26361	**0.82652 ± 0.011639**	0.81687 ± 0.068966	0.63538 ± 0.20789	0.55533 ± 0.26903	0.61872 ± 0.22181
5	0.7087 ± 0.1898	0.80897 ± 0.096959	0.76942 ± 0.17734	0.68495 ± 0.21275	0.5133 ± 0.22502	0.52963 ± 0.27783	0.81293 ± 0.082849	0.82332 ± 0.090118	0.79204 ± 0.14222	0.69342 ± 0.21084	0.75478 ± 0.17458
6	0.7013 ± 0.1482	0.84656 ± 0.013572	**0.85152 ± 0.011037**	0.82612 ± 0.10087	0.60783 ± 0.20261	0.71186 ± 0.18971	0.84831 ± 0.009557	0.85013 ± 0.015255	0.8366 ± 0.074204	0.74983 ± 0.16564	0.82406 ± 0.016708
7	0.7011 ± 0.1387	0.79025 ± 0.043927	0.74545 ± 0.12743	0.65289 ± 0.16991	0.49256 ± 0.19726	0.49798 ± 0.21703	0.78996 ± 0.01552	**0.79335 ± 0.057861**	0.77142 ± 0.099999	0.66094 ± 0.18496	0.7225 ± 0.13606
8	0.5292 ± 0.1950	0.76646 ± 0.1227	0.74727 ± 0.161	0.5946 ± 0.2163	0.43324 ± 0.21718	0.47473 ± 0.24354	**0.7696 ± 0.12937**	0.76865 ± 0.14446	0.73408 ± 0.18322	0.52876 ± 0.23229	0.73028 ± 0.17976
9	0.6272 ± 0.1967	0.7794 ± 0.084019	0.74133 ± 0.12806	0.64587 ± 0.2152	0.54463 ± 0.22665	0.55877 ± 0.24081	**0.80807 ± 0.044904**	0.75203 ± 0.12024	0.70729 ± 0.18519	0.65695 ± 0.20145	0.77316 ± 0.11388
10	0.7771 ± 0.1393	0.80422 ± 0.12585	0.83831 ± 0.11098	0.79496 ± 0.16331	0.60229 ± 0.22154	0.54115 ± 0.22649	0.82791 ± 0.078231	**0.87179 ± 0.021505**	0.79322 ± 0.16314	0.62317 ± 0.21718	0.67625 ± 0.18646
11	0.6834 ± 0.2219	**0.80511 ± 0.092076**	0.77442 ± 0.14977	0.62232 ± 0.25091	0.55453 ± 0.28157	0.58034 ± 0.28575	0.80409 ± 0.048416	0.80372 ± 0.099851	0.80229 ± 0.15517	0.65624 ± 0.24172	0.75813 ± 0.1044
12	0.6533 ± 0.2100	0.74389 ± 0.16522	0.74755 ± 0.18315	0.63992 ± 0.23159	0.53068 ± 0.22636	0.52352 ± 0.22507	0.75723 ± 0.15195	**0.7632 ± 0.16064**	0.72508 ± 0.19973	0.56365 ± 0.22998	0.70295 ± 0.2021
13	0.7851 ± 0.1158	0.87473 ± 0.055109	0.86971 ± 0.041848	0.83028 ± 0.1472	0.6639 ± 0.24207	0.73632 ± 0.2266	0.8784 ± 0.031997	**0.87951 ± 0.029392**	0.87816 ± 0.065242	0.79958 ± 0.17007	0.82529 ± 0.090573
14	0.7183 ± 0.1617	0.8552 ± 0.015434	0.85809 ± 0.024329	0.82058 ± 0.12098	0.68155 ± 0.1803	0.70816 ± 0.17964	**0.86109 ± 0.023652**	0.85788 ± 0.023947	0.8101 ± 0.11521	0.70902 ± 0.17323	0.83512 ± 0.044322
15	0.7358 ± 0.1854	**0.86625 ± 0.017805**	0.85847 ± 0.066214	0.73814 ± 0.20304	0.61491 ± 0.24517	0.65481 ± 0.26258	0.85201 ± 0.013346	0.85533 ± 0.044846	0.84986 ± 0.1029	0.74037 ± 0.21502	0.82972 ± 0.12797
16	0.7990 ± 0.1614	0.81633 ± 0.040866	0.81921 ± 0.052318	0.73385 ± 0.1747	0.5909 ± 0.23776	0.64237 ± 0.22922	0.81769 ± 0.03101	0.82269 ± 0.018116	**0.8307 ± 0.074**	0.7814 ± 0.15654	0.79847 ± 0.076856
FINAL	0.6956 ± 0.0707	0.8042 ± 0.1012	0.7921 ± 0.1332	0.7002 ± 0.2102	0.5601 ± 0.2418	0.5856 ± 0.2530	0.8115 ± 0.0826	**0.8132 ± 0.0994**	0.7831 ± 0.1522	0.6682 ± 0.2219	0.7513 ± 0.1582

Img	ASM	$ASMLBP_{8,1}$	$ASMLBP_{8,2}$	$ASMLBP_{8,3}$	$ASMLBP_{8,5}$	$ASMLBP_{8,10}$	$ASMLBP^{med}_{8,1}$	$ASMLBP^{med}_{8,2}$	$ASMLBP^{med}_{8,3}$	$ASMLBP^{med}_{8,5}$	$ASMLBP^{med}_{8,10}$
1	4.133 ± 2.0244	3.2832 ± 1.1684	3.1533 ± 0.82827	3.8834 ± 1.7948	5.2248 ± 2.6375	5.5638 ± 3.0434	3.0528 ± 0.5405	**3.0255 ± 0.56206**	3.3026 ± 1.0745	4.5689 ± 2.3776	4.1828 ± 2.2844
2	3.2091 ± 0.8171	2.9125 ± 1.1658	**2.6767 ± 0.79874**	2.9271 ± 1.0362	3.7974 ± 1.9718	3.4667 ± 1.9125	2.8358 ± 1.0838	2.7416 ± 0.85442	2.7685 ± 0.95405	3.1156 ± 1.2837	2.929 ± 1.4363
3	3.6292 ± 1.5555	**2.6831 ± 0.75415**	3.1923 ± 1.9965	3.6941 ± 2.1727	6.0888 ± 2.3291	5.3907 ± 2.2679	2.6867 ± 0.70532	3.2449 ± 2.0108	2.8682 ± 1.3829	4.9483 ± 2.2386	5.1756 ± 2.5223
4	4.8023 ± 2.2745	2.8974 ± 0.78172	3.2382 ± 1.4378	4.9401 ± 2.21	6.3231 ± 2.5616	5.6395 ± 2.6231	**2.7439 ± 0.29996**	2.9335 ± 0.958	4.7145 ± 2.0902	5.5351 ± 2.5026	4.9911 ± 2.4504
5	4.1877 ± 2.3050	3.2118 ± 1.2285	3.5311 ± 1.6237	4.5618 ± 2.531	7.4603 ± 3.0776	7.7669 ± 4.3206	3.1109 ± 0.88929	**3.0253 ± 0.85514**	3.394 ± 1.7213	4.6552 ± 2.9041	3.9011 ± 2.7682
6	3.4692 ± 1.6640	3.117 ± 0.30008	3.079 ± 0.27943	3.1057 ± 0.84793	5.3829 ± 2.2647	4.9597 ± 3.0086	3.1437 ± 0.31039	**2.9948 ± 0.25406**	3.1967 ± 0.72601	4.0088 ± 2.1306	3.0816 ± 0.27995
7	3.7034 ± 1.4986	3.0979 ± 0.4829	3.5314 ± 1.3349	4.8783 ± 2.1668	6.8017 ± 2.1764	6.2205 ± 2.4304	**3.0128 ± 0.41394**	3.064 ± 0.67867	3.3451 ± 1.0851	4.35 ± 2.0383	3.7256 ± 2.1547
8	5.7813 ± 2.6944	3.3611 ± 1.7202	3.6502 ± 2.1625	5.7231 ± 2.9962	7.4596 ± 2.5295	7.8326 ± 3.5353	**3.1879 ± 1.3466**	3.9376 ± 3.2345	3.9552 ± 2.7799	6.5143 ± 3.0993	4.3505 ± 3.5996
9	5.0035 ± 2.5482	3.1757 ± 1.2994	3.9853 ± 2.1543	5.282 ± 2.9372	6.1726 ± 2.6847	6.246 ± 3.0995	**2.7729 ± 0.68053**	3.7346 ± 1.974	4.5324 ± 2.6597	5.0383 ± 2.5179	3.4337 ± 1.5014
10	4.2112 ± 2.1171	3.6596 ± 1.4147	3.4608 ± 1.1721	3.9324 ± 1.5011	6.138 ± 2.3331	7.3214 ± 2.9103	3.2991 ± 0.84516	**3.068 ± 0.26908**	4.0152 ± 1.912	5.8396 ± 2.4792	4.909 ± 2.5771
11	4.1633 ± 2.6696	4.0044 ± 1.0381	4.2655 ± 1.3982	5.6093 ± 2.0539	6.3346 ± 2.5045	6.5629 ± 3.0882	3.8799 ± 0.5154	4.1747 ± 1.4233	4.1022 ± 1.3315	5.2869 ± 2.2604	**3.7975 ± 1.2464**
12	6.3160 ± 1.7137	3.8 ± 2.2834	3.7413 ± 2.0414	4.8446 ± 2.5674	6.0858 ± 2.4399	6.785 ± 2.9258	3.7296 ± 2.1684	**3.5809 ± 1.9108**	4.0986 ± 2.5607	5.8084 ± 2.7002	4.2629 ± 2.8437
13	2.7991 ± 1.2834	2.4505 ± 0.83002	2.3312 ± 0.59566	2.9055 ± 1.5506	4.9694 ± 2.6755	4.1011 ± 2.8692	2.348 ± 0.4421	**2.3146 ± 0.43819**	2.4878 ± 0.89705	3.1576 ± 1.8783	2.5186 ± 1.0781
14	4.2416 ± 1.4517	**2.637 ± 0.15443**	2.6714 ± 0.24235	2.9769 ± 1.0622	4.4829 ± 1.946	4.4335 ± 2.5588	2.6829 ± 0.24502	2.7018 ± 0.26753	3.0583 ± 1.1088	4.2827 ± 1.8584	2.762 ± 0.79662
15	3.7797 ± 2.2689	2.5607 ± 0.23371	2.6861 ± 0.76326	4.2698 ± 2.3158	5.619 ± 2.5146	5.9532 ± 3.8202	**2.5002 ± 0.14624**	2.647 ± 0.68231	2.7644 ± 1.1075	4.2281 ± 2.4094	3.0849 ± 1.9181
16	3.6147 ± 2.1238	2.7895 ± 0.67022	2.8499 ± 0.76479	3.9409 ± 1.9885	6.0137 ± 2.9605	5.855 ± 3.5376	2.7794 ± 0.47206	**2.775 ± 0.35317**	2.9011 ± 0.9668	3.617 ± 2.1557	2.9868 ± 1.3533
FINAL	4.1903 ± 0.9152	3.1943 ± 1.3026	3.3628 ± 1.5467	4.4207 ± 2.3522	6.1084 ± 2.6847	6.1737 ± 3.3362	**3.0709 ± 1.0552**	3.2007 ± 1.4841	3.5348 ± 1.8453	4.8029 ± 2.5759	3.8071 ± 2.3367

Table 3. Mean and standard deviation of DICE (top) and HAUSDORFF DISTANCE (below) results for each image of dataset.